FINITE ELEMENT MODELING OF FLUID-STRUCTURE INTERACTION OF AN ELASTIC 2D FLAG IN HARMONIC VISCOUS FLUID FLOW AND OF AN ELASTIC 3D SAIL STRUCTURE IN STATIONARY VISCOUS FLUID FLOW (CONCISED VERSION)

CARSTEN CORTE

Baustatik – Baudynamik – Numerische Modellierung
Thrasoltstraße 12, 10585 Berlin, Tel. / Fax +49-(0)30-347 871 78 / 80

Abstract. A fully consistent finite element model for fluid-structure interaction between incompressible viscous fluids and elastic structures considering large structural deformation is presented. The coupling approach is based on a segregated solution procedure for the Navier-Stokes equations for incompressible viscous fluid flow and the structural equation of motion for elastic structures.

The fluid-structure interaction model is applied on the 2D example of a rigid and elastic, respectively, flag in the quasi-harmonic fluid wake flow behind a square rigid obstacle. Time-harmonic pattern of fluid flow and time-harmonic structural deformation are evaluated at different steps of oscillation. Transient evolution of acting coupling forces on the common fluid-structure interface is shown and pointed out.

The fluid-structure interaction model is further applied on the 3D example of a rigid and elastic, respectively, mast and sail structure that is exposed to quasi-stationary fluid flow on its surface. Corresponding structural response is analyzed with respect to different stages of fluid-structure coupling that can be applied to finally arrive at the fully consistent stage of the fluid-structure interaction model. Characteristics of fluid flow pattern and deformation of mast and sail structure are pointed out.

The concised version only shows evaluation of computational results.

CONTENT

Development of numerical methods on structural mechanics (e.g. Clough [1], Craig [2], Bathe [3]), fluid mechanics (e.g. Brooks and Hughes [4], Pantakar [5], Anderson [6], Zienkiewicz [7]) and on fluid-structure interaction (e.g. Wall [8], Walhorn [9], Hübner [10], Hübner et al. [11], Corte et al. [12], [13], Corte [14]) aims as main intention to find an answer to the general problem of fluid-structure interaction, to develop a general solution approach that covers the representation of different fields of fluid-structure interaction for different length scales and different time scales. Corte [15], [16] shows a detailed evaluation of a 3D fluid-structure interaction approach (segregated; time domain modeling) that couples the Navier-Stokes equations (incompressible viscous fluids) with the general structural dynamics equation (elastic structures) regarding large structural deformation. Corte [20], [21] develops a 3D membrane theory (consistent spatial finite element discretization, finite difference time discretization, time domain modeling of 3D membrane dynamics) and applies it to a wide-span elastic 3D membrane roof structure considering 3D viscous fluid flow around the membrane roof structure (Corte [22]).

In the applied fluid structure-interaction computational approach both fluid domain and structural domain are discretized by 3D hexahedral elements with trilinear interpolation functions. On the fluid side the Euler backward scheme and on the structural side the HHT-α scheme (Hilber et. al. [17]) are applied for time discretization.

Fig. 2: fluid x-velocity over
time (rigid 2D flag)
Fig. 3: velocity magnitude at
t=248.1 s (rig. 2D flag)

Fig. 4: fluid x-velocity over
time (elastic 2D flag)
Fig. 5: velocity magnitude at
t=56.1 s (el. 2D flag)

Fig. 7: y-displacement at
x=0.50L, x=1.00L over time
Fig. 6: fluid-structure
iterations over timestep index

Fig. 7: y-components of
$\mathbf{f}_{F,n+1}^{FSI,int}$, $\mathbf{Grad}_{F,n+1}^{old}\mathbf{p}_{F,n+1}^{old}$
Fig. 7: $\mathbf{f}_{presF,n+1}$ (y-directed)
at x=0.50L over time

Fig. 8: y-components of
$\mathbf{f}_{F,n+1}^{FSI,int}$, $\mathbf{Grad}_{F,n+1}^{old}\mathbf{p}_{F,n+1}^{old}$
Fig. 8: $\mathbf{f}_{presF,n+1}$ (y-directed)
at x=1.00L ov. time

Rigid and elastic 2D flag in harmonic viscous flow

The example of a rigid and elastic, respectively, 2D flag (L = 4 m length (x), 0.06 m width (y), 0.1 m height (z)) behind a square rigid obstacle (B = 1 m side length (x, y), 0.1 m height (z), center located 6 m downstream of fluid inflow boundary) in surrounding harmonic viscous flow is shown by a 3D fluid domain (25.5 m length (x), 12 m width (y), 0.1 m height (z)). The fluid domain is discretized by 20944 nodes and 10200 hexahedral elements in x-y flow plane. The structural 2D flag domain is discretized by 410 nodes and 160 hexahedral elements in x-y flow plane (80 structural element layers in x-direction and two structural element layers in y-direction), one element layer is used in z-direction (both fluid and structure).

Fluid density 1000 kg/m³, kinematic viscosity is 5 kg/(m·s). Inflow velocity (vel_{Fx}, vel_{Fy}, vel_{Fz}) is (1 m/s, 0, 0), Reynolds number Re = 200 around the square rigid obstacle. Structural density is 1000 kg/m³, Poisson's ratio is 0.0, modulus of elasticity is 21000 N/m². Time domain integration time interval size is 0.1 s, HHT- α parameter α = -0.1. Time domain computation is carried out with rigid 2D flag (initial 300 s total time) and with elastic 2D flag (another 75 s total time).

For rigid 2D flag oscillation period of the fluid pattern is ≈9.09 s, frequency is ≈0.110 Hz (fig. 2), fig. 3 shows velocity magnitude pattern at t = 248.1 s. For elastic 2D flag the fluid mesh is only deformed in y-direction (lateral). Fluid mesh velocity for a certain fluid node is defined as the difference of the fluid mesh deformation of that node at the current timestep and at the previous timestep divided by the time interval size. Oscillation period of the fluid pattern is ≈9.29 s, frequency is ≈0.108 Hz (fig. 4), fig. 5 shows velocity magnitude pattern at t = 56.1 s. A slight decrease in oscillation frequency can be pointed out in comparison to the solely fluid flow with a rigid 2D flag. Decrease in frequency for the coupled fluid-structure system appears because the elastic flag contributes an additional amount of mass to be accelerated by the fluid where the fluid is the only energy delivering part in this specific fluid-structure system (through constant velocity inflow at fluid inflow boundary). In comparison to the flow pattern around rigid 2D flag (fig. 2, fig. 3) fluid pattern is obviously more irregular and amplitudes of fluid velocity (fig. 4, fig. 5) and fluid pressure are clearly higher for the case of elastic 2D flag. Nevertheless average values of fluid velocity and pressure at the corresponding positions are roughly the same for both cases of rigid and elastic 2D flag.

For elastic 2D flag period of the structural oscillation (≈9.29 s, frequency ≈0.108 Hz) is the same as of surrounding fluid field; the elastic 2D flag is mutually coupled with the surrounding fluid flow, {≈9.29 s; ≈0.108 Hz} is the common oscillation {period; frequency} of the coupled fluid-structure interaction system.

Focus on the coupled force equilibrium on the fluid-structure interface leads to augmented equations for both the fluid problem and the structural problem. $\mathbf{f}_{F,n+1}^{FSI,int}$ is the fluid force that acts on the structure on the fluid-structure interface. At this point, a distinction between i) $\mathbf{f}_{F,n+1}^{FSI,int}$, ii) the part $\mathbf{Grad}_{F,n+1}^{old}\mathbf{p}_{F,n+1}^{old}$ of $\mathbf{f}_{F,n+1}^{FSI,int}$ and iii) the direct normal force $\mathbf{f}_{presF,n+1} = \int_{\Gamma_{F,n+1FSI}} \mathbf{p}_{F,n+1}^{old} \, d\Gamma_{F,n+1}^{FSI}$ due to fluid pressure on the fluid-structure interface is made ($\Gamma_{F,n+1}^{FSI}$: fluid structure interface $\subset$ fluid boundary). By evaluation of y-components of i) $\mathbf{f}_{F,n+1}^{FSI,int}$, ii) $\mathbf{Grad}_{F,n+1}^{old}\mathbf{p}_{F,n+1}^{old}$ and iii) $\mathbf{f}_{presF,n+1}$ at positions x = 0.50L, y = {- ; +}0.03B and x = 1.00L, y = {- ; +}0.03B on both lateral sides of the 2D flag it becomes obvious from figs. 7 and 8 that the direct normal force $\mathbf{f}_{presF,n+1}$ is much bigger than y-components of $\mathbf{f}_{F,n+1}^{FSI,int}$ and $\mathbf{Grad}_{F,n+1}^{old}\mathbf{p}_{F,n+1}^{old}$, respectively. Particularly the sum of nodewise force values from both lateral sides (which is the accelerating quantity on the 2D flag in y-direction) is much bigger for $\mathbf{f}_{presF,n+1}$ than it is for $\mathbf{f}_{F,n+1}^{FSI,int}$ and $\mathbf{Grad}_{F,n+1}^{old}\mathbf{p}_{F,n+1}^{old}$, respectively; especially at x = 0.50L sum of nodewise force $\mathbf{f}_{presF,n+1} \in [\approx$-2.5 N; $\approx$2.1 N], whereas {$\mathbf{f}_{F,n+1}^{FSI,int}$; $\mathbf{Grad}_{F,n+1}^{old}\mathbf{p}_{F,n+1}^{old}$} $\in [\approx$-0.02 N; $\approx$0.02 N] (fig. 7), at x = 1.00L $\mathbf{f}_{presF,n+1} \in [\approx$-0.9 N; $\approx$0.8 N] and {$\mathbf{f}_{F,n+1}^{FSI,int}$; $\mathbf{Grad}_{F,n+1}^{old}\mathbf{p}_{F,n+1}^{old}$} $\in [\approx$-0.7 N; $\approx$0.6 N] (fig. 8).

For to remind: For results presented here within the computation $\mathbf{f}_{F,n+1}^{FSI,int}$ (fluid force on structure) and vice versa $\mathbf{f}_{S,n+1}^{FSI,int}$ (structural force on fluid) is applied. This is in contrast with several other works on fluid-structure interaction. Wall [8], Hübner [11], Zibouche [18] and Corte [13], [14] deal with the example of an elastic 2D flag in viscous flow, Gallinger [19] with an elastic 2D flag with rigid circular cylinder.

In Wall [8], Hübner [11], Zibouche [18] and Gallinger [19] (only) fluid pressure and fluid viscous stress and (only) elastic structural stress are faced with each other. Corte [12], [14] shows application of fluid-structure interaction on the 3D case of vortex shedding around a 3D elastic circular cylinder.

Wall [8], Hübner [11] and Zibouche [18] use fluid density to structural density relation of $\rho_F / \rho_S = 1.8 \cdot 10^{-2}$ [8], $5.9 \cdot 10^{-4}$ [8], [11] and $6.125 \cdot 10^{-4}$ [18] which represents very light weight fluids in comparison to the corresponding structure. Oscillation amplitudes of y-displacement obtained are 0.012 m [8], 0.0075 m [8], 0.008 m and 0.02 m (two different cases) [11] with therein used 2D flag length of 0.04 m. Time interval sizes used are no data [8], 0.001 s [11], 0.01 s [18]. A larger oscillation amplitude of 0.4 m y-displacement is obtained ($\rho_F / \rho_S = 6.125 \cdot 10^{-4}$, [18]) with 2D flag length of 4 m, also modeling a relatively light weight fluid. Corte [13], [14], applying an $\mathbf{f}_{F,n+1}^{FSI,int}$ and an $\mathbf{f}_{S,n+1}^{FSI,int}$, models a rather heavy weight fluid ($\rho_F / \rho_S = 1.0$) and obtains y-displacement oscillation amplitude of 0.41 m with 2D flag length of 4 m, time interval size used is 0.1 s. Here, in this work ($\rho_F / \rho_S = 1.0$), with application of $\mathbf{f}_{F,n+1}^{FSI,int}$ and $\mathbf{f}_{S,n+1}^{FSI,int}$ maximum y-displacement oscillation amplitude of 0.18 m is obtained, time interval size 0.1 s, see above. Gallinger [19] (elastic 2D flag, circular cylinder) obtains y-displacement of 0.083 m ($\rho_F / \rho_S = 0.1$) and 0.037 m ($\rho_F / \rho_S = 1.0$) with 2D flag length of 0.35 m, time interval sizes 0.00025 s, 0.0010 s.

Further, Gallinger [19] points out that convergence behaviour in general becomes worse in case fluid density and structural density become similar, i.e. in case the mass of the fluid that moves with the structure in the vicinity of the structure increases.

An explanation on Gallinger's beforehand statement **and** an **appropriate remedy** is given here:

Particularly for *transient* fluid-structure problems, where *large* structural deformations appear and therefore a *large* velocity of the fluid-structure interface can appear, i.e. where acceleration forces due to the fluid mass in the vicinity of the structure affect the state of the elastic structure *noticeably* and where mutually acceleration forces due to the structural mass on the fluid in the vicinity of the structure affect the state of the incompressible viscous fluid *noticeably*, convergence problems naturally appear in case acceleration forces from the fluid on the structure

are neglected and in case acceleration forces from the structure on the fluid are neglected. And in case only fluid pressure force (normal to the fluid-structure interface) and fluid shear force (viscous fluid force) are applied on the structure on the fluid-structure interface and in case only elastic structural force (from structural stress inducing structural strain) is applied on the fluid on the fluid-structure interface *then* acceleration forces (fluid mass forces and structural mass forces) and fluid convective forces

are simply completely neglected on the fluid-structure interaction interface. Exemplarily the big difference between forces considering acceleration components ($\mathbf{f}_{F,n+1}^{FSI,int}$) and neglecting acceleration components ($\mathbf{f}_{presF,n+1}$ only) on the fluid-structure interface can obviously be seen in fig. 7 and can also be seen in fig. 8. In case normal pressure force $\mathbf{f}_{presF,n+1}$ were applied on the structure to describe force equilibrium on the fluid-structure interface (see figs. 7 and 8) then structural displacement would be determined to be much larger than it does by application of $\mathbf{f}_{F,n+1}^{FSI,int}$ on the fluid-structure interface (figs. 7 and 8); the larger structural displacement would in turn lead to higher pressure in the fluid; this mechanism finally lets the solution process of the coupled fluid-structure interaction problem diverge. Such an experience has been made by Corte [14] for the 3D case of vortex shedding around a 3D elastic circular cylinder, where structural acceleration forces are *not* applied on the fluid on the fluid-struture interface. Therein a solution for a long-term simulation (2000 time intervals) could still be obtained for a fluid to structural density relation of $\rho_F / \rho_S = 5.0 \cdot 10^{-4}$ (where high frequency oscillations of fluid pressure and structural velocity could be observed towards the end of the modeled simulation time) with a relatively light weight fluid whereas for the fluid to structural density relation of $\rho_F / \rho_S = 5.0 \cdot 10^{-3}$ a relatively heavier weight fluid was modeled and divergence of the coupled solution process appeared at a very early stage of the simulation (after 170 time intervals) with very high amplitude high frequency oscillations of fluid pressure and structural velocity [14]. For the third case of a relatively most light weight fluid (fluid to structural density relation of $\rho_F / \rho_S = 5.0 \cdot 10^{-5}$) exponential increase of high frequency oscillation amplitude over simulation time could be observed for fluid pressure and structural velocity with regularity [14]; divergence of the solution process for this third case appeared after 1075 time intervals of simulation [14].

As completion, as shown here in this work, consideration of $\mathbf{f}_{F,n+1}^{FSI,int}$ and $\mathbf{f}_{S,n+1}^{FSI,int}$ in the discrete form of force equilibrium of the coupled fluid-structure interation problem completes the consistent discrete form of force equilibrium of the coupled fluid-structure interation problem; this discrete form is independent of considered length scale to be modeled and independent of considered time scale to be modeled and consistent with arbitrary ranges of material parameter relations that appear with the considered fluid-structure interaction case to be modeled and is consistent with the time interval size to be applied.

In the concised version attention is drawn to entrance of $\mathbf{f}_{S,n+1}^{FSI,int}$ into fluid continuity equation in its discretized form by spatial divergence operator, $\mathbf{Div}_{F,n+1}^{old}$. Deep evalu-/derivation of this consistent approach to model fluid-structure interaction is given in Corte [16].
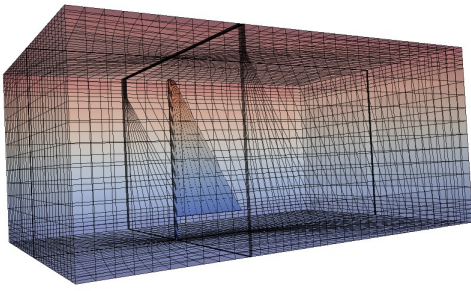
Fig. 9: 3D computational fluid domain with structural mast and sail
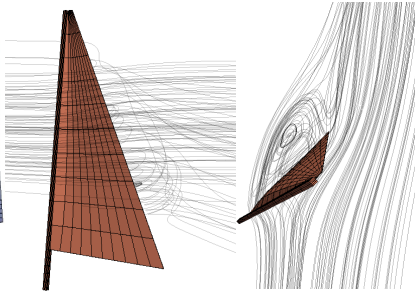
Fig. 12: sideview and groundview on stream-lines of fluid flow around rigid structure
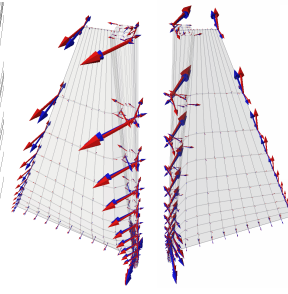
Fig. 14: fluid-structure inter-action forces $\mathbf{f}_{F,n+1}^{FSI,int}$ (red), $\mathbf{Grad}_{F,n+1}^{old}\mathbf{p}_{F,n+1}^{old}$ (blue) on elastic mast and sail
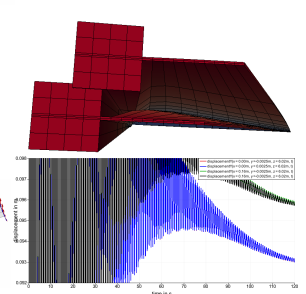
Fig. 15: elastic mast, sail: undeformed,deformed state
Fig. 16: y-displac'm. of up-, downstream sail top ov.tm.

Rigid and elastic 3D sail in stationary viscous flow

The example of a rigid and elastic, respectively, 3D sail (quadrangular shape with 6.02 m luff length (z), 3.35 m foot length (x), 0.16 m head length (x), shape with maximum leeward extension of 0.154 m at 0.479 m from luff, 1.81 m above foot and leeward extension of 0.156 m at 0.412 m from luff, 2.41 m above foot, foot fixed in displacement, sail thickness 0.005 m) and rigid and elastic, respectively, mast in surrounding stationary viscous fluid flow is shown. Mast length is 7.02 m (quadratic cross-section, edge length 0.1 m, mast fixed in displacement at its bottom, mast bottom at z = -1.00 m), sail ranges from z = 0.00 m to z = 6.02 m. Mast and sail have material properties density ρ_S = 1000 kg/m³, Poisson's ratio ν_S = 0.0 and modulus of elasticity E_S = 1.5·10⁶ N/m². Fluid domain has 18 m length (x), 12 m width (y) and 8 m height (z). Fluid density is ρ_F = 1000 kg/m³, kinematic viscosity is μ_F = 5 kg/(m·s). Inflow velocity (vel_{Fx}, vel_{Fy}, vel_{Fz}) is 2/3 m/s·(cos(35°), sin(35°), 0) at upstream boundary (x) and windward lateral boundary (y) (angle 35° is from x-axis). Pressure is zero at downstream boundary. Mast is positioned 6 m from upstream boundary (x). Fluid domain is discretized by 32760 nodes and 29360 hexahedral elements. Structure (mast and sail) is discretized by 890 nodes and 560 hexahedral elements (thereof sail: 10 (height, z) × 10 (length, x) × 2 (thickness, y) elements), fig. 9. Time domain integration time interval size is Δt = 0.1 s, HHT-α parameter α = -0.33. As a stationary state is expected for the coupled fluid-structure problem and as for this 3D case the fluid mesh is quite coarse (fig. 9) no fluid mesh deformation is performed during the computation to avoid oscillations on the fluid solution due to a moving-in-time fluid domain. The (finally stationary) fluid state is computed considering structural forces $\mathbf{f}_{S,n+1}^{FSI,int}$ on the fluid but is computed on the undeformed fluid mesh. The (finally stationary) structural state is computed considering $\mathbf{f}_{F,n+1}^{FSI,int}$ on the structure.

First, mast and sail are considered as rigid. Stationary fluid state is obtained by fluid inflow velocity stepwise 0.1 m/s·(cos(35°), sin(35°), 0) for 35 time intervals, then 1/3 m/s·(cos(35°), sin(35°), 0) for another 165 time intervals, then 2/3 m/s·(cos(35°), sin(35°), 0) for another 1000 time intervals. The stationary flow field around the rigid sail structure is vizualized by streamlines in fig. 12; a typical vortex in the flow field can be seen leeward from the sail. Second, mast and sail are considered as elastic. Fluid inflow velocity is 2/3 m/s·(cos(35°), sin(35°), 0) for 1200 time intervals (Δt = 0.1 s). Fluid velocity state and fluid pressure state do not change appreciably compared with the case for rigid mast and sail. Deformed shape of elastic mast and sail is shown in fig. 15. Deformation is clearly oriented leewards and downstream. Lateral structural displacement (y) of upstream top (x = 0.00 m, y = {- ; +}0.0025 m, z = 6.02 m) and downstream top (x = 0.16 m, y = {- ; +}0.0025 m, z = 6.02 m) of the sail (fig. 16) is ≈0.093 m at x = 0.00 m and ≈0.096 m at x = 0.16 m, showing a relative leeward displacement of the downstream sail top of 0.003 m compared with the upstream sail top. Stationary state distribution of nodewise forces $\mathbf{f}_{F,n+1}^{FSI,int}$ and $\mathbf{Grad}_{F,n+1}^{old}\mathbf{p}_{F,n+1}^{old}$ that act on elastic mast and sail can be seen in fig. 14. It can be

noted that $\mathbf{f}_{F,n+1}^{FSI,int}$ that acts on the structure appears the largest on geometric edges, on mast and leech, whereas $\mathbf{f}_{F,n+1}^{FSI,int}$ on the inner of the sail surface and on the inner of the mast surface appears comparatively very small. Nodewise contribution $\mathbf{Grad}_{F,n+1}^{old}\mathbf{p}_{F,n+1}^{old}$ of $\mathbf{f}_{F,n+1}^{FSI,int}$ has about 90 percent magnitude of the corresponding $\mathbf{f}_{F,n+1}^{FSI,int}$ as can be estimated from fig. 14. In the stationary solution mass and acceleration effects do not play any role, so (100 - 90) percent = 10 percent of the fluid-structure interaction forces $\mathbf{f}_{F,n+1}^{FSI,int}$ are associated with viscous fluid shear forces and convective fluid forces. For two selected positions (downstream top of the sail at x = 0.16 m, z = 6.02 m, windward and leeward side, and at maximum leeward extension of the sail at x = 0.412 m , z = 2.41 m, windward and leeward side) a comparison of y-components of both $\mathbf{f}_{F,n+1}^{FSI,int}$ and $\mathbf{Grad}_{F,n+1}^{old}\mathbf{p}_{F,n+1}^{old}$ and nodewise normal pressure force $\mathbf{f}_{presF,n+1} = {}_{\Gamma F,n+1FSI}\int \mathbf{p}_{F,n+1}^{old} d\Gamma_{F,n+1}^{FSI}$ is listed in table 1. At downstream top of the sail (x = 0.16 m, z = 6.02 m) y-components of the two forces $\mathbf{f}_{F,n+1}^{FSI,int}$ in total (sum) and $\mathbf{Grad}_{F,n+1}^{old}\mathbf{p}_{F,n+1}^{old}$ in total (sum) both clearly are directed leewards. In contrast the normal pressure force $\mathbf{f}_{presF,n+1}$ in total (sum) on the fluid-structure interface is directed windwards and comparatively small in magnitude. As the stationary solution is not affected by fluid mass forces (fluid acceleration is zero) most of the force action is associated with $\mathbf{Grad}_{F,n+1}^{old}\mathbf{p}_{F,n+1}^{old}$ and only (100 - 100·9.460/10.105) = 6.4 percent is associated with viscous and convective fluid forces at this position. So it can be concluded that the spatial derivative of the fluid pressure with respect to y-direction in the vicinity of the downstream sail top plays the major role for fluid-structure interaction force equilibrium at the downstream sail top. At position with maximum leeward exension of the sail (x = 0.412 m, z = 2.41 m) y-components of the two forces $\mathbf{f}_{F,n+1}^{FSI,int}$ in total (sum) and $\mathbf{Grad}_{F,n+1}^{old}\mathbf{p}_{F,n+1}^{old}$ in total (sum) as well as the normal pressure force $\mathbf{f}_{presF,n+1}$ in total (sum) are all clearly directed leewards. As the stationary solution is not affected by fluid mass forces (fluid acceleration is zero) most of the force action is associated with $\mathbf{Grad}_{F,n+1}^{old}\mathbf{p}_{F,n+1}^{old}$ and only (100 - 100·1.172/1.188) = 1.3 percent is associated with viscous and convective fluid forces at this position. Y-components of $\mathbf{f}_{F,n+1}^{FSI,int}$ in total (sum) and $\mathbf{Grad}_{F,n+1}^{old}\mathbf{p}_{F,n+1}^{old}$ in total (sum) are small compared with the corresponding values at the downstream sail top position (x = 0.16 m, z = 6.02 m). It can be concluded that the spatial derivative of fluid pressure with respect to y-direction at the considered position (x = 0.412 m, z = 2.41 m) is appropriately smaller than the spatial derivative of fluid pressure with respect to y-direction at the downstream sail top position (x = 0.16 m, z = 6.02 m) which is comprehensible because the fluid state windward of the sail structure is much more regular than it is around the leech of the sail structure (see fig. 12 (fluid flow field around rigid structure)). Normal pressure force $\mathbf{f}_{presF,n+1}$ in total (sum) at position x = 0.412 m, z = 2.41 m is much bigger than y-components of the two forces $\mathbf{f}_{F,n+1}^{FSI,int}$ in total (sum) and $\mathbf{Grad}_{F,n+1}^{old}\mathbf{p}_{F,n+1}^{old}$ in total (sum). Application of $\mathbf{f}_{presF,n+1}$ to formulate the coupled force equilibrium on the fluid-structure interface would lead to much higher structural deformation at the appropriate position of the sail structure which in turn could affect fluid pressure increase in the vicinity of the sail which then can possibly lead to nonconvergence of the respective coupled solution approach.

position (x, y, z)	$[\mathbf{f}_{F,n+1}^{FSI,int}]Y$	$[\mathbf{Grad}_{F,n+1}^{old}\mathbf{p}_{F,n+1}^{old}]Y$	$\mathbf{f}_{presF,n+1}(Y)$
0.160 m, -0.0025 m, 6.02 m 0.160 m, +0.0025 m, 6.02 m	19.646 N (leeward) -9.541 N (windward)	19.006 N (leeward) -9.546 N (windward)	-0.035 N (windward) 0.067 N (windward)
SUM	10.105 N (leeward)	9.460 N (leeward)	0.102 N (windward)
0.412 m, +0.1535 m, 2.41 m 0.412 m, +0.1585 m, 2.41 m	-0.671 N (windward) 1.859 N (leeward)	-0.698 N (windward) 1.870 N (leeward)	25.28 N (leeward) -16.23 N (leeward)
SUM	1.188 N (leeward)	1.172 N (leeward)	41.51 N (leeward)

Table 1: y-components of both nodewise forces $\mathbf{f}_{F,n+1}^{FSI,int}$ and $\mathbf{Grad}_{F,n+1}^{old}\mathbf{p}_{F,n+1}^{old}$ and normal pressure force $\mathbf{f}_{presF,n+1}$ (here acting approximately in y-direction) at selected positions of sail structure on fluid-structure interface (downstream sail top and position of maximum leeward extension of sail)

REFERENCES

[1] Clough, R. W. 1975: Dynamics of structures. McGraw-Hill, New York
[2] Craig, R. R. 1981: Structural dynamics: an introduction to computer methods. Wiley, New York
[3] Bathe, K.-J. 1996: Finite-Elemente-Methoden. Springer-Verlag, Berlin
[4] Brooks, A. N., Hughes, T. J. R. 1982: Streamline upwind/Petrov-Galerkin formulations for the convection dominated flows with particular emphasis on the incompressible Navier-Stokes equations. Computer methods in applied mechanics and engineering, vol. 32, **199-259**
[5] Pantakar, S. V. 1980: Numerical heat transfer and fluid flow. Hemisphere publications, New York
[6] Andersen, J. D. 1995: Computational fluid dynamics. McGraw-Hill, New York
[7] Zienkiewicz, O. C. 2000: Fluid dynamics. The finite element method, vol. 3, Butterworths-Heinemann, Oxford
[8] Wall, W. A. 1998: Fluid-Struktur-Interaktion mit stabilisierten finiten Elementen. Institut für Baustatik, Universität Stuttgart
[9] Walhorn, E. 2002: Ein simultanes Berechnungsverfahren für Fluid-Struktur-Wechselwirkungen mit finiten Raum-Zeit-Elementen. Institut für Statik, Technische Universität Braunschweig
[10] Hübner, B. 2003: Simultane Analyse von Bauwerk-Wind-Wechselwirkungen. Institut für Statik, Technische Universität Braunschweig
[11] Hübner, B., Walhorn, E., Dinkler, D. 2004: A monolithic approach to fluid-structure interaction using space-time finite elements. Computer methods in applied mechanics and engineering, vol. 193 (23-26), **2087-2104**
[12] Corte, C., García, J., Oñate, E. 2007: Three-dimensional flow around rigid and elastic cylindrical structures. CIMNE Barcelona, **32 pages**
[13] Corte, C., García, J., Oñate, E. 2008: A strongly coupled segregated approach for finite element modeling of fluid-structure interaction. CIMNE Barcelona, **17 pages**
[14] Corte, C. 2008: A segregated approach for strong coupling of finite element solvers to model fluid-structure interaction. CIMNE Barcelona, **30 pages**
[15] Corte, C. 2010: A 3D approach for finite element modeling of viscous fluid flow. Dr. Corte Ingenieurbüro für Bauwesen, Berlin, **24 pages**
[16] Corte, C. 2011: A 3D approach for finite element modeling of fluid-structure interaction between viscous fluids and elastic structures. Dr. Corte Ingenieurbüro für Bauwesen, Berlin, **64 pages**
[17] Hilber, H. M., Hughes, T. J. R., Taylor, R. L. 1977: Improved numerical dissipation for time integration algorithms in structural dynamics. Earthquake engineering and structural dynamics, vol. 5, **283-292**
[18] Zibouche, K., Mounajed, G., Dupuy, J. M. 2005: Fluid-structure interaction with large displacements modeling in civil engineering: Application to slender structures, tall buildings subjected to turbulent wind flows. EURODYN 2005, Paris, vol. 2, **1373-1378**
[19] Gallinger, T. G. 2011: Effiziente Algorithmen zur partitionierten Lösung gekoppelter Probleme der Fluid-Struktur-Wechselwirkung. Technische Universität München
[20] Corte, C. 2014: 3D-Membrantheorie. Der Stahlbau 83 Heft 5, **343-358**
[21] Corte, C. 2014: 3D membrane theory. World congress on computational mechanics WCCM XI 2014, Barcelona, **268-292**
[22] Corte, C. 2017: Membrane roof structures. STRUCTURAL MEMBRANES 2017, Technische Universität München, **478-502**